CHAPTER 1

Tycho's Six: High Resolution spectroscopy search for the donor of the Tycho supernova

This Chapter is being prepared for publication as 'Tycho's Six: High-Resolution spectroscopy search for the donor of the Tycho supernova' - Kerzendorf, W. E., Schmidt, B. P., Yong, D., Jeffery, C.S. , Anderson, J.P., Nomoto, K., Podsiadlowski, Ph., Simon, J.D., Gal-Yam, A., Silverman, J.M., Filipenko, A.V., Murphy, S.J., Bessell, M.S.

1.1. Introduction

Type Ia supernovae (SNe Ia) are of great interest for astronomy. They represent some of the most extreme physical situations in stellar astronomy, produce substantive amounts of iron group element (IGE) which impacts the chemical evolution of galaxies and the Universe, and are uniquely powerful cosmic distance probes. Despite their wide ranging significance, fundamental uncertainties remain around the progenitor of these cataclysmic events.

There is general consensus that SNe Ia are caused by the deflagration/detonation of a CO-WD which is accreting material from a binary companion. Scenarios exists where the explosion can be initiated from a detonation on the surface of the star (Livne & Arnett, 1995; Fink et al., 2010), through runaway carbon burning in the white dwarf's interior, or through a cataclysmic merger of objects.

Observationally, two main scenarios for this accretion process can be identified. The single degenerate scenario (SD-scenario) sees the accretion process occurring through Roche Lobe Overflow (RLOF) of a close non-degenerate companion (also known as donor star). This companion, which has undergone common envelope evolution with the white dwarf, can be a helium, main-sequence, sub-giant, or red giant star. In all cases the donor star should survive the explosion (except for possibly in the case of the helium star donor; priv. comm. Rüdiger Pakmor) and remains visible post-explosion.

The second scenario is the dynamical merger of two white dwarfs (double degenerate scenario (DD-scenario)). In this scenario, the co-evolution of two stars eventually leads to

a close binary of two white dwarfs, which are able, through the emission of gravitational radiation, to merge over a wide range of times after the initial formation of the system. In most cases this would leave no remaining star (e.g. Pakmor et al., 2010).

Both scenarios have support in observation and theory. The detection of circumstellar material around certain SN Ia such as SN 2006X (Patat et al., 2007), provides support for the SD-Scenario. On the other hand the lack of substantial hydrogen in the majority of other SNe Ia (Leonard, 2007) poses a challenge to the SD-Scenario.

Kasen (2010) suggests that the interaction with the non-degenerate companion should imprint an observable signature on a SN Ia light curve, depending on viewing angle, and radius of the companion. Such an excess has not yet been observed (Hayden et al., 2010; Tucker, 2011; Bianco et al., 2011) which is at odds with red giant companions forming the majority of SNe Ia.

Population synthesis calculations are challenging, with various authors getting different results for the same inputs (e.g. Nelemans, 2010). However there is a general trend from these calculations that neither single-degenerate nor double degenerate stars can provide enough systems to explain the SN Ia rate (Ruiter et al., 2009; Mennekens et al., 2010; Yu & Jeffery, 2010; Han, 2008). Several authors suggest the population might comprise both single and double degenerate systems.

The physics of white dwarf mergers is challenging to simulate numerically, but in the simplest calculations, these mergers will lead to the formation of a neutron star via an electron capture, rather than a thermonuclear explosion (Saio & Nomoto, 1985). Recently Pakmor et al. (2010) have shown that for certain parameters (white dwarf binaries with a mass ratio very close to one) the merger may explain sub-luminous supernovae (e.g. 91bg-like SNe Ia), although Dan et al. (2011) note that the initial conditions of the system may change these conclusions.

To investigate the nature of progenitors observationally Ruiz-Lapuente et al. (2004) (RP04) have tried to directly detect donor stars in SN Ia remnants within the Milky Way. They have identified two historical Galactic SNe well suited to this task - SN 1006 and SN 1572 (Tycho's SN). Both remnants are young (440 and 1000 years old, respectively), almost certainly SN Ia from both their observational signatures (Badenes et al., 2006; Ruiz-Lapuente, 2004) and not overwhelmed by Galactic extinction. In this paper, we will focus on SN 1572.

SNR 1572 is relatively close (2.8 ± 0.8 kpc), very young and has been confirmed as a normal SN Ia remnant both from the remnant (Badenes et al., 2006) and from a light echo (Krause et al., 2008; Rest et al., 2008).

RP04 investigated most bright stars in the central regions of SN 1572 and found a star with an unusual spatial motion (Tycho-G by their nomenclature) and suggested this as a possible donor star for SN 1572. While the star has an unusual spatial motion compared to other stars in the field, its current location and proper motion place it a significant distance from the remnant's center - a feature difficult to explain in connecting Tycho-G to SNR 1572. One consequence of RLOF is a rotational velocity induced on the donor star by tidal locking in the system. This results in an unusually large rotationally velocity, related to the orbital velocity of the binary system and can be used to single out donor stars against nearby unrelated stars. Kerzendorf et al. (2009) (WEK09) investigated rotation for Tycho-G but found no excess rotation velocity compared to a normal star. WEK09's measurements of Tycho-G, including a revised radial velocity, compared to Galactic kinematic models

showed it is statistically consistent with an interloping star. However, WEK09 were able to provide an a priori unlikely scenario, where the star was able to lose its rotational signature.

González Hernández et al. (2009) (GH09) analysed a spectrum of Tycho-G observed with the High Resolution Echelle Spectrometer (HIRES; Vogt et al., 1994) instrument on the Keck telescope. In addition to confirming WEK09's radial velocity for Tycho-G, GH09 measured its stellar parameters and metallicity. GH09 concluded that Tycho-G has an unusually large amount of nickel. GH09 claim that this enhancement in nickel can be attributed to the accretion of ejecta material on the donor star during the explosion.

In this paper we analyse HIRES spectra of the six bright stars in SNR 1572 center. These spectra were taken by the same program that obtained the data used by GH09 and we independently reanalyze this spectrum as part of our program. We describe the observational data and our data reduction procedures in Section 1.2. Section 1.3 is divided into five subsections detailing the measurements of proper motion, radial velocity, rotation, stellar parameters and abundances. In Section 1.4 we analyse the measurements of each star to investigate its potential association with SNR 1572, and present our conclusion in Section 1.5.

1.2. Observations and Data Reduction

We obtained spectra with the HIRES on the Keck 10m telescope on Mauna Kea. The observations were made on two nights on 2006 September 10 and 2006 October 11. The slits B5 and C1 (with the same width of 0.86'' but different lengths, B5 length 3.5'', C1 length 7.0'') were used resulting in a wavelength coverage of 3930–5330 Å, 5380–6920 Å and 6980–8560 Å with $R \approx 50,000$, providing us with the necessary spectral resolution and wavelength coverage to determine stellar parameters. The spectra were reduced using the MAKEE package. All spectra were corrected to heliocentric velocities, using the MAKEE skyline method. The spectra were not corrected for telluric lines as they will not influence our analysis of the stellar parameters. The final exposure times of the combined spectra for each candidate and signal to noise ratio at 4000-4100 Å are shown in Table 1.1. Finally we normalized the spectrum using the IRAF[1] task CONTINUUM. We note that Tycho-C and Tycho-D were observed on the same slit (C1) with a separation of 2.1''.

[1]IRAF: the Image Reduction and Analysis Facility is distributed by the National Optical Astronomy Observatory, which is operated by the Association of Universities for Research in Astronomy (AURA) under cooperative agreement with the National Science Foundation (NSF).

Table 1.1 Observations of Stars

Tycho	RA (J2000) (hh:mm:ss.ss)	Dec (J2000) (dd:mm:ss.ss)	Date (dd/mm/yy)	Slit	t_{exp} (s)	S/N
A	00:25:19.73	+64:08:19.60	10/09/06	B5	900	≈ 65
B	00:25:19.95	+64:08:17.11	10/09/06	B5	1200	≈ 50
C	00:25:20.40	+64:08:12.32	11/10/06	C1	10800	≈ 10
D	00:25:20.60	+64:08:10.82	11/10/06	C1	10800	≈ 5
E	00:25:18.29	+64:08:16.12	11/10/06	C1	9000	≈ 15
G	00:25:23.58	+64:08:02.06	10/09/06 & 11/10/06	B5&C1	24000	≈ 30

In addition, we obtained low-resolution spectroscopy ($R \approx 1200$) of Tycho-B with the dual-arm Low-Resolution Imaging Spectrometer (LRIS; Oke et al., 1995) mounted on the 10-m Keck I telescope. The observations were taken on one run on 2010 November 07, using only the blue arm with the 600/4000 grism and the 1'' wide slit. This resulted in a wavelength coverage of 3200 – 5600 Å. These observations were taken to obtain a precise measurement of the surface gravity for Tycho-B using the size of the Balmer decrement (Bessell, 2007). The spectrum of Tycho-B was reduced using standard techniques (e.g. Foley et al., 2003). Routine CCD processing and spectrum extraction were completed with IRAF, and the data were extracted with the optimal algorithm of Horne (1986). We obtained the wavelength scale from low-order polynomial fits to calibration-lamp spectra. Small wavelength shifts were then applied to the data after measuring the offset by cross-correlating a template sky to the night-sky lines that were extracted with the star. Using our own IDL routines, we fit a spectrophotometric standard-star spectrum to the data in order to flux calibrate Tycho-B and remove telluric lines (Horne, 1986; Matheson et al., 2000).

1.3. Analysis

1.3.1. Astrometry

Proper motions can be used to identify potential donor stars because donor stars freely travel with their orbital velocity after the SN explosion disrupts the system. RP04 suggested Tycho-G as a possible donor due to its unusually high proper motion and unusually high radial velocity. For this work we measured proper motions for 201 stars within one arcminute of the remnant's centre. We used archival HST images for three different epochs (HST Program ID 9729 & 10098; November 2003, August 2004, May 2005) each consisting of three exposures (1 s, 30 s and 1440 s) in the F555W using the Advanced Camera for Surveys (ACS). The pixel size in each exposure is 50 mas pixel^{-1}. This dataset results in a maximum baseline of 30 months.

We used an image from the middle epoch (2004) to establish a reference frame and oriented the pixel coordinate system with the equatorial system. We then applied a distortion correction for the F555W filter (Anderson & King, 2006) to each images and then calculated transformations between all other images and the reference image. We then used these transformations to calculate the position of all stars in the reference coordinate system with the overall uncertainty of each position estimated. Some faint stars where not detected in the shorter exposures and were thus excluded from proper motion measurements (with 114 Stars remaining).

For each star, we fit a linear regression for the stellar positions over time in the pixel coordinates (which were aligned with the equatorial system). The x and y data were treated as independent measurements, with separate regressions solved for each axis directions. Errors were estimate using standard least squares analysis and the individual error estimates each object's positions.

There are three measurements of the geometric center of SN 1572 using different datasets. Reynoso et al. (1997) using Very Large Array (VLA) data measured the center to $\alpha = 00^h25^m14\overset{s}{.}95$ $\delta = +64°08'05.7''$ J2000, Hughes (2000) using ROSAT data measured $\alpha = 00^h25^m19\overset{s}{.}0$ $\delta = +64°08'10''$ J2000 and Warren et al. (2005) with Chandra data measured

Table 1.2 Proper motion of Candidates

Tycho	RA (J2000) (hh:mm:ss.ss)	Dec (J2000) (dd:mm:ss.s)	μ_α	μ_δ	$\Delta\mu_\alpha$	$\Delta\mu_\delta$	r
			mas yr^{-1}		mas yr^{-1}		$''$
B	0:25:19.97	64:08:17.1	-1.24	0.56	0.62	0.64	4.86
A	0:25:19.73	64:08:19.8	-0.09	-0.89	1.17	0.90	6.21
A2	0:25:19.81	64:08:20.0	-0.71	-3.60	0.69	0.64	6.58
C	0:25:20.38	64:08:12.2	-0.21	-2.52	0.65	0.65	6.66
E	0:25:18.28	64:08:16.1	2.04	0.54	0.66	0.69	7.60
D	0:25:20.62	64:08:10.8	-1.12	-1.99	1.01	0.86	8.60
1	0:25:16.66	64:08:12.5	-2.27	-1.37	1.60	1.15	18.00
F	0:25:17.09	64:08:30.9	-4.41	0.20	0.70	0.71	22.69
J	0:25:15.08	64:08:05.9	-2.40	-0.25	0.62	0.62	29.44
G	0:25:23.58	64:08:01.9	-2.50	-4.22	0.60	0.60	29.87
R	0:25:15.51	64:08:35.4	0.28	0.24	0.89	0.80	33.23
N	0:25:14.73	64:08:28.1	1.18	0.89	0.86	0.98	33.66
U	0:25:19.24	64:07:37.9	0.01	-3.04	0.73	0.75	36.06
Q	0:25:14.81	64:08:34.2	1.45	3.07	0.64	0.72	36.19
T	0:25:14.58	64:07:55.0	-3.85	0.52	0.72	0.62	36.78
K	0:25:23.89	64:08:39.3	0.18	0.17	0.73	0.69	38.73
L	0:25:24.30	64:08:40.5	0.16	-0.44	0.75	0.82	41.59
S	0:25:13.78	64:08:34.4	4.16	0.58	0.83	0.84	42.09
2	0:25:22.44	64:07:32.4	74.85	-4.43	0.82	0.83	46.09

the center to $\alpha = 00^h25^m19\overset{s}{.}40$ $\delta = 64°08'13.98''$ J2000.

Table 1.2 lists the proper motions and errors of all stars mentioned in RP04 (19 stars) which were analyzed in this work as well as the distance to the geometric X-ray center measured by Chandra.

We compared the distribution of proper motions of all measured stars to ours candidates in Figure 1.1.

1.3.2. Radial Velocity

The radial velocity of each star was measured using the IRAF task FXCOR (Tonry & Davis, 1979). MAKEE was used to calculate an intrinsic velocity shift by comparing offsets of the nightsky-lines. The radial velocity standards were reduced in the same fashion.

Each order of each star was then cross-correlated with at least two other radial velocity standards (HR6349, HR6970 & HR1283) which had been observed on the same night.

The radial velocity for Tycho-B was measured in the course of determining the stellar parameters for Tycho-B with the stellar parameter fitting package SFIT. The SFIT result consistently gives $v_{\rm helio} = -55$ km s^{-1} for different stellar parameters with an error of ≈ 2 km s^{-1}.

In Table 1.3 we have listed all the radial velocities both in a heliocentric frame and a *local standard of rest* (LSR) frame. We will be referring to the heliocentric measurements from here on. The listed error is the standard deviation of the radial velocity measurement

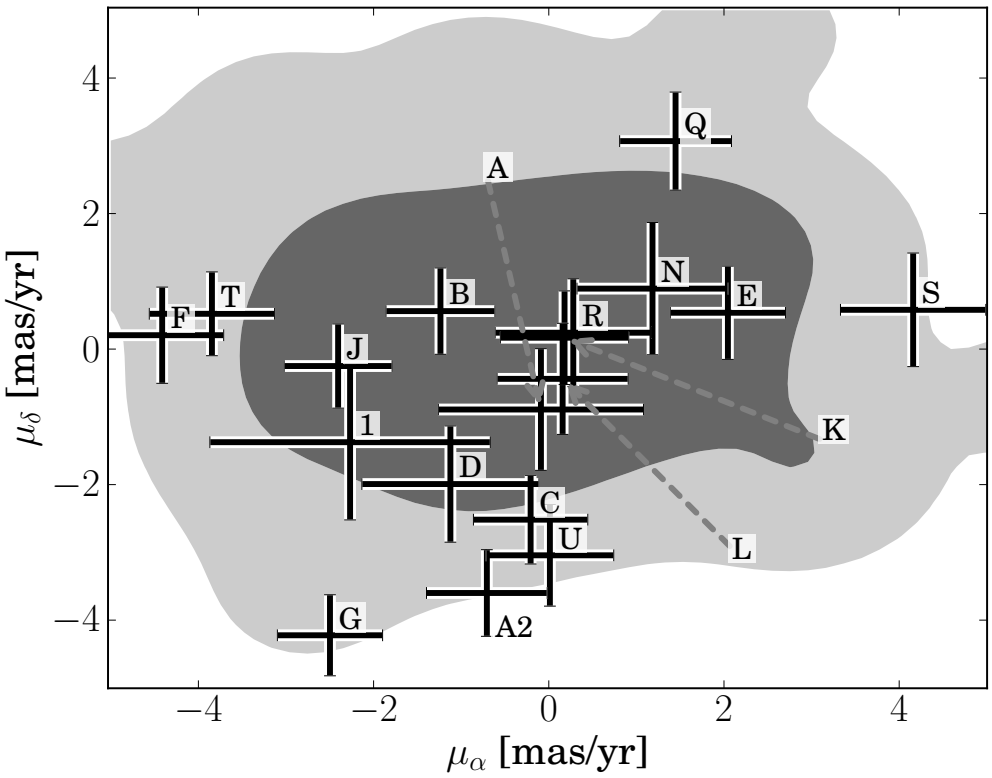

Figure 1.1 The contours show the distribution of proper motions (68% and 95% probability) for all stars measured towards the Tycho SNR - excluding the named stars. We show the location of the candidate stars and their errors on top of this distribution. Tycho-2 was not shown in this figure as it is an extreme outlier with $\mu_\alpha = 75\,\mathrm{mas\,yr^{-1}}$ and $\mu_\delta = -4.4\,\mathrm{mas\,yr^{-1}}$ but also at a large distance to the center of the remnant's geometric center (46″).

of all orders added in quadrature to the error of the radial velocity standards.

In Figure 1.2 we have compared the radial velocity of our sample stars to radial velocities of stars in the direction of Tycho's SNR using the Besançon Model (Robin et al., 2003). The distance as well as the error in distance are taken from Section 1.3.5. The candidates radial velocities are all typical for their distance. Finally, we note the measurement of Tycho-G is consistent with WEK09 and GH09.

1.3.3. Rotational Velocity

We have measured rotational velocities of all stars except Tycho-B in the same fashion as described in WEK09. We selected several unblended and strong (but not saturated) Fe I lines in the stellar spectra . We added these lines after shifting them to the same wavelength and scaling them to the same equivalent width (EW). This was done to improve the S/N ratio for the faint stars as well as providing consistency throughout all stars.

As a reference we created three synthetic spectra for each star (one broadened only with the instrumental profile, the others with the instrumental profile and $v_{\mathrm{rot}} \sin i$ of 10 and 13 km s^{-1} respectively) with the 2010 version of MOOG (Sneden, 1973), using our derived temperature, gravity and metallicity. As input data to MOOG we used the Castelli & Kurucz

Table 1.3 Radial velocities

Name designation	Date (dd/mm/yy)	$v_{\rm helio}$ (km s^{-1})	$v_{\rm LSR}$ (km s^{-1})	Δv (km s^{-1})
Tycho-A	09/09/06	-36.79	-28.5	0.23
Tycho-B	09/09/06	-55.0	-57.0	≈ 2
Tycho-C	11/10/06	-58.78	-50.49	0.75
Tycho-D	11/10/06	-58.93	-50.64	0.78
Tycho-E	11/10/06	-64.2	-55.91	0.27
Tycho-G	09/09/06	-87.12	-78.83	0.25
Tycho-G	11/10/06	-87.51	-79.22	0.78

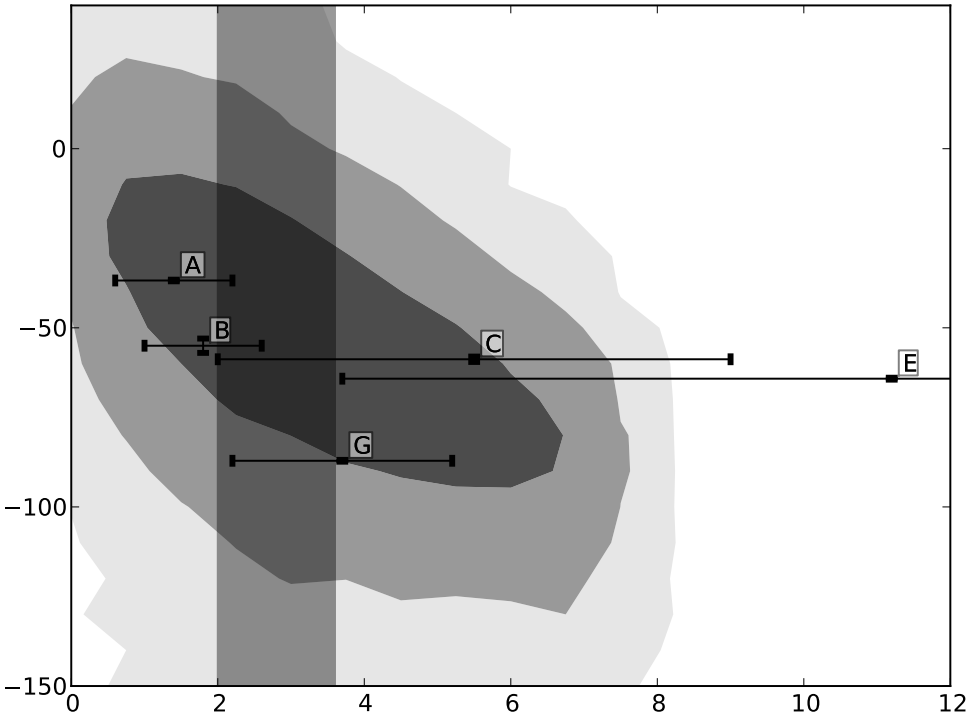

Figure 1.2 The contours indicate 1, 2 and 3 $-\sigma$ levels of the distance and radial velocity using the Besançon Model (Robin et al., 2003) with $\approx 60,000$ stars in the direction of SN 1572 (only including stars with $10 < V < 20$ and stars with a metallicity of [Fe/H] > -1). We have over plotted our candidate stars with error bars. One should note that the errors in distance are a marginalised approximate of the error, the proper error surfaces can be seen in Figure 1.6. The vertical gray shade shows the error range for the distance of SNR1572.

(2004) atmospheric models and a line list from Kurucz & Bell (1995). We then applied the same process of line selection and adding as for the lines in the observed spectra.

Figure 1.3 shows the comparison between the synthetic spectra of different rotational velocity and the observed spectra. This comparison indicates that the stellar broadening (rotational, macro turbulence, etc.) is less than broadening due to the instrumental profile

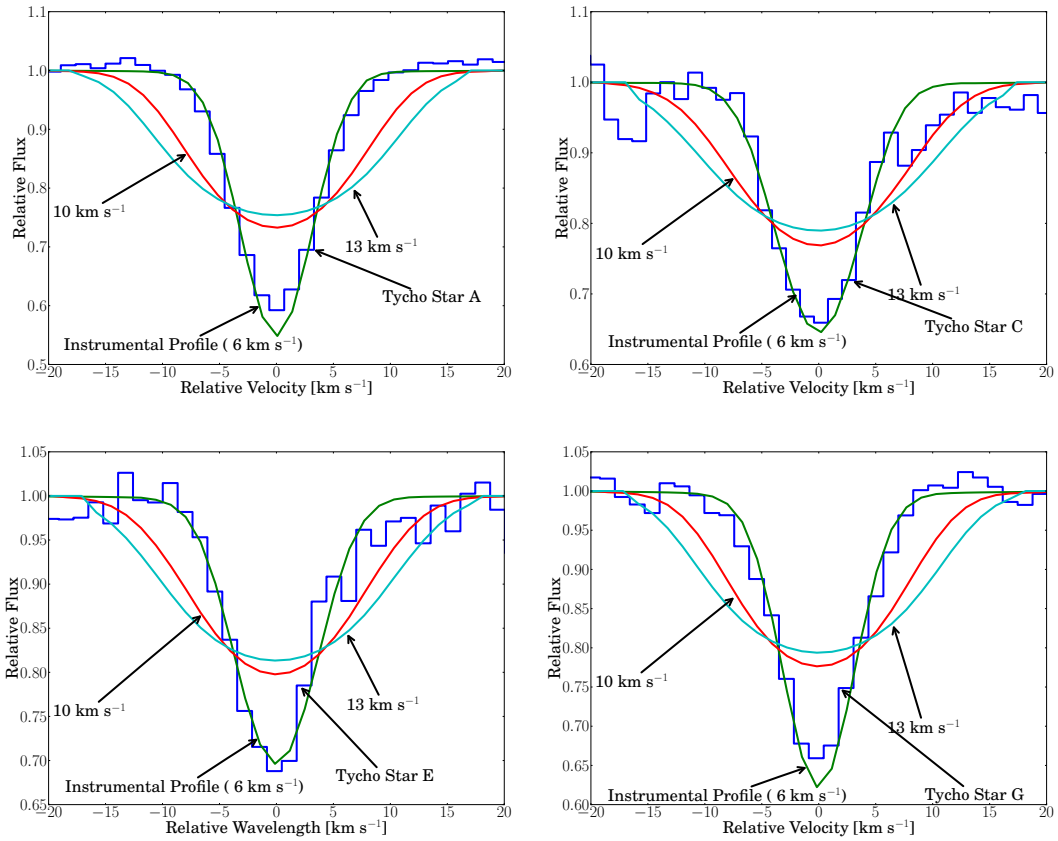

Figure 1.3 The figures show the combination of iron line profiles after normalization to the same Equivalent Width and compare them to synthetic line profiles created by MOOG. We convolved the synthetic lines first with a rotational kernel with three different values for rotation and then with the instrumental profile. All stars show rotation less than 6 km s^{-1} which is equal to the instrumental profile at this resolution.

of 6 km s^{-1} for each star. We adopt 6 km s^{-1} as an upper limit to the rotation for all stars.

Due to its high temperature and rotation, we fit the rotational velocity for Tycho-B with the program SFIT (Jeffery et al., 2001, described in section 1.3.4) as part of the overall fit for this star's stellar parameters. We find $v_{\rm rot} = 171^{+16}_{-33}$ km s^{-1}. While Tycho-B's rotation is very high compared to the other candidate stars, for stars of this temperature and gravity a high rotation is not unusual. In summary, other than Tycho-B, none of the stars show rotation which is measurable at this resolution.

1.3.4. Stellar parameters

The stellar parameters are presented in Table 1.4 and were determined using a traditional spectroscopic approach based on the EWs of lines of different excitation and ionization levels. . These measurements exclude Tycho-B, due to its hot temperature, and we measure its stellar parameters by direct comparison to models, in a separate procedure.

EWs for a set of iron lines were measured using routines in IRAF (compiled from Reddy et al. (2003, henceforth Reddy03) and Ramírez & Cohen (2002, henceforth RC02) Table 1.5 shows the EWs measured for each of the stars. Missing values indicate that the line was

Table 1.4 Stellar Parameters

Name designation	$T_{\rm eff}{}^a$ (K)	$\log g^b$ (dex)	[Fe/H] (dex)	Δ[Fe/H] (dex)	[Ni/H] (dex)	Δ[Ni/H] (dex)	[Li/H] (dex)
Tycho-A	4975	2.9	0.02	0.16	0.025	0.1	0.09
Tycho-C	4950	2.9	-0.57	0.23	-0.17	0.14	0.11
Tycho-E	5825	3.4	-0.16	0.21	0.0	0.2	0.131
Tycho-G	6025	4	-0.15	0.18	0.08	0.14	0.11

[a] $\sigma_{T_{\rm eff}} \approx 100$ K
[b] $\sigma_{\log g} \approx 0.3$ dex

not detected.

We used the *local thermodynamic equilibrium* (LTE) stellar line analysis program MOOG and LTE model atmospheres from the Castelli & Kurucz (2003) grid to derive an abundance for a given line. The effective temperature was adjusted until the abundances from Fe I lines displayed no trend as a function of excitation potential. The surface gravity was adjusted until the abundances from Fe I and Fe II lines were in agreement. The microturbulent velocity, ξ_t , was adjusted until there was no trend between the abundances from the Fe I lines and EW. This process was iterated until self consistent stellar parameters were obtained for each star. In our analysis, we explored stellar parameters at discrete values. For effective temperature, we considered values at every 25 K (e.g. 4000, 4025 K, etc.), for surface gravity , we considered values at every 0.05 dex (e.g., 1.00, 1.05 dex, etc.), and for ξ_t , we considered values at every 0.05 km s^{-1}(e.g. 1.70, 1.75 km s^{-1}, etc.). We assumed that excitation equilibrium was satisfied when the slope between $\log \epsilon$(Fe I) and lower excitation potential (χ) was ≤ 0.004. We assumed that ionization equilibrium was achieved when $|\log \epsilon(\text{Fe I}) - \log \epsilon(\text{Fe II})| \leq 0.02$ dex. The microturbulent velocity was set when the slope between $\log \epsilon$(Fe I) and reduced EW ($\log W/\lambda$) was ≤ 0.004. In all cases we found appropriate solutions in which the trends between Fe I, Fe II, EWs and excitation potentials were small. We estimate that the internal errors are typically $T_{\rm eff}$, ±100 K, $\log g \pm 0.3$ dex, and $\xi_t \pm 0.3$ km s^{-1}. For further details regarding the derivation of stellar parameters, see Yong et al. (2008).

The final iron measurements are the average of Fe I and Fe II assuming the solar abundances of Asplund et al. (2009) In addition, we measured abundance for the Elements nickel and lithium via EW analysis. We could not see any unusual abundance pattern for any of the sample stars (see Figure 1.4; Tycho-B's abundances are not presented on the plot as they were measured in a different fashion).

In summary, the inferred metallicities for all candidates show that the candidates are of roughly solar metallicities with the exception of the metal-poor Tycho-C. The range of metallicities spanned by the program stars is compatible with membership of the thin disk. Based on metallicity alone, we do not regard any of the program stars to be unusually metal-poor or metal-rich. Additionally, we find the [Ni/Fe] abundance to be consistent with stars of similar metallicity (see Figure 1.4). The stellar paramaters and elemental abundances are listed in Table 1.4.

Because Tycho-B has a temperature greater than 9000 K and is quickly rotating, the process described above cannot be used to measure stellar parameters. Instead we used the program SFIT to match the HIRES spectrum to a grid of model spectra. To determine

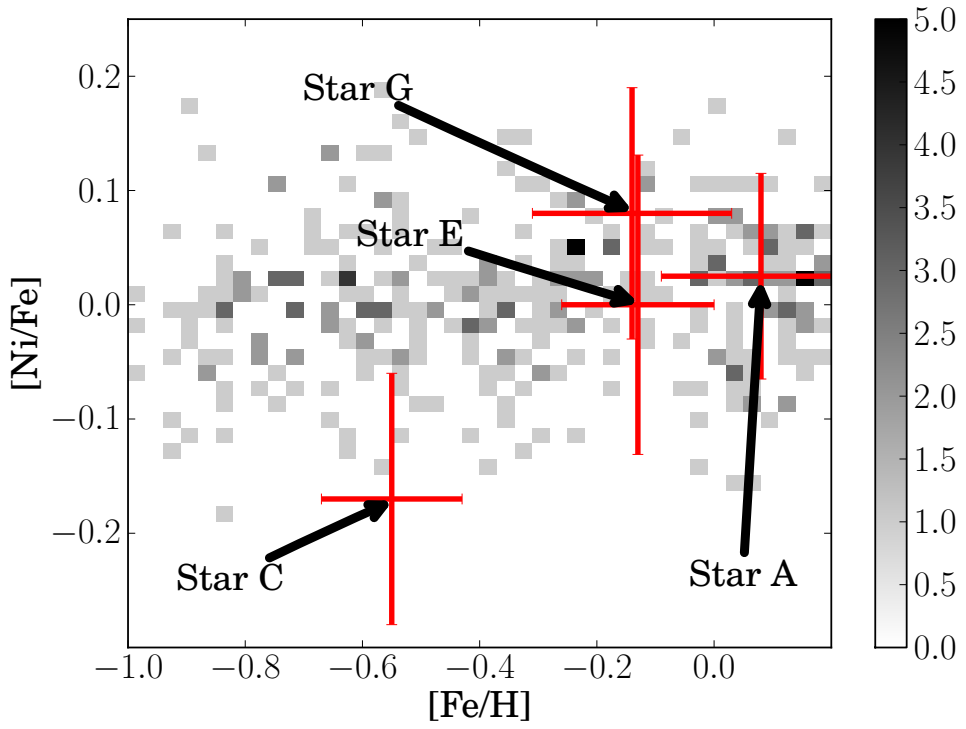

Figure 1.4 The background colour indicates the distribution is taken from Kobayashi et al. (2006). All of the measured candidates are consistent within the errors with stars of the same metallicity.

the stellar parameters for Tycho-B we have used a model grid with [Fe/H] = −1.0, 8000 < $T_{\rm eff}$ < 16000, 7 < $\log g$ < 2. This low metallicity is suggested by a very weak Calcium K line and Mg II lines, but is hard to measure. We can not measure Helium directly in this spectrum and thus adopt N(He) = 0.1 as this is empirically a very common Helium abundance in stars.

This analysis resulted in $T_{\rm eff} = 10000^{+400}_{-200}$ K, $\log g = 3.67$ with slope $\partial \log g / \partial T_{\rm eff} = 0.27/500\,{\rm K}^{-1}$, rotational velocity $v_{\rm rot} \sin i = 171\,{\rm km\,s}^{-1}$ with slope $\partial v_{\rm rot} \sin i / \partial T_{\rm eff} = -41/500\,{\rm km\,s}^{-1}\,{\rm K}^{-1}$. From qualitative analysis this object seems metal poor (e.g. in comparison to stars of similar stellar parameters but solar metallicity), but its high rotation and temperature make it hard to determine this parameter precisely. For the present, we assume [Fe/H] = -1.0 unless otherwise noted.

In addition, using the high-resolution spectrum, we measured the EWs of several lines predicted to be strong in the Vienna Atomic Line Database (VALD; Kupka et al., 2000). The abundances were deduced from the EWs using a model atmosphere having $T_{eff} = 10000$ K, $\log g = 3.67$ and [Fe/H] = -1.0 (see Table 1.6).

One caveat regarding these abundances is the use of EWs from single lines with large rotational broadening, since the effect of blending with nearby weak lines cannot be taken into account. A second is that these abundances invariably rely on the strongest lines, which are precisely those most susceptible to departures from LTE. Nevertheless, they do confirm the earlier impression that the star is metal-poor, and justify the adoption of [Fe/H]=−1.0 ± 0.4.

As a second approach to determine the stellar parameters of Tycho-B we used the

low resolution spectra observed with LRIS. The observation range of LRIS was chosen to be centred around the Balmer jump as this feature is sensitive to the surface gravity (Bessell, 2007). We fitted the spectra to a grid of model spectra (Munari et al., 2005) using a spectrum fitting tool described below. The final grid we used covered $\log g$ from 3.5 to 4.5 in steps of 0.5 and effective temperature from 9000 to 12000 K in steps of 500 K. In addition we expanded the grid by reddening the spectra with the PYSYNPHOT[2] package. We also added diffuse interstellar bands (Beals & Blanchet, 1937; Herbig, 1966, 1967, 1975, 1995; Hibbins et al., 1994; Jenniskens & Desert, 1994; Wilson, 1958) to the synthetic spectra which were scaled with reddening. The included E(B-V) ranged from 0.5 to 1.3 in steps of 0.2. We assumed a rotation of 171 km s^{-1} in the grid (see section 1.3.3).

We used χ^2 as a figure of merit in our fitting procedure. To find the best fit for Tycho-B we used the MIGRAD algorithm provided by MINUIT and linearly interpolated between the grid points using LINEARNDINTERPOLATOR provided by the SCIPY package (see Appendix **??** for a more detailed description of the interpolation process). The fit of Tycho-B results in $T_{\rm eff}$=10570 K, $\log g$=4.05, [Fe/H]=-1.1 and E(B-V)=0.85. The model fits the synthetic spectrum poorly in the wavelength region between 3800 – 4280 Å in (see Figure 1.5). The adopted mixing length parameter used in 1D model atmospheres, used to construct the spectral grid, influences the fluxes in that region as well as affecting the hydrogen line profiles. Heiter et al. (2002) and others show that a mixing length of 0.5, rather than 1.25 as used in the Kurucz/Munari grid, better fits the violet fluxes and the hydrogen line profiles. Spectra using a mixing length parameter of 0.5 are brighter in the ultra violet (UV) and the H_γ, H_δ and H_β profiles give the same effective temperature as the Hα profiles. We have chosen, however, to fit the spectrum and ignore the problematic spectral region (3800 – 4280 Å) to avoid a systematic error. This yields $T_{\rm eff}$ = 10722 K, $\log g$ = 4.13,[Fe/H] = −1.1 and E(B-V)=0.86. The differences are indicative of the size of systematic errors in the model fits. We adopt the fit excluding the problematic wavelength region in the further analysis. Exploring the complex search space we estimate the error to be $\Delta T_{\rm eff}$ = 200 K, $\Delta\log g$=0.3 and Δ[Fe/H]=0.5, and note that the parameters are correlated.

1.3.5. Distances

To measure the distance to the candidate stars we used colours and absolute magnitude from isochrones by Pietrinferni et al. (2004). We used the MIGRAD algorithm (James & Roos, 1975) to find close matches of the measured values to $T_{\rm eff}$-$\log g$ isochrones by varying the age of the isochrone. Subsequently we calculate E(B-V) using the isochrone's colour and we extract a mass from the isochrone. The results can be seen in Table 1.7. To estimate the errors in all distance, reddening and mass we employed the *Monte Carlo* (MC) method with 10,000 samples of effective temperature , surface gravity, metallicity, B- and V-magnitude (see Figure 1.6). Errors included in Table 1.7 are the standard deviations of the Monte-Carlo sample. The data shows that all stars are compatible with the distance of the remnant. This is not unexpected as the uncertainties of the measurements in stellar parameters are relatively large.

pos

[2]pysynphot is a product of the Space Telescope Science Institute, which is operated by AURA for NASA.

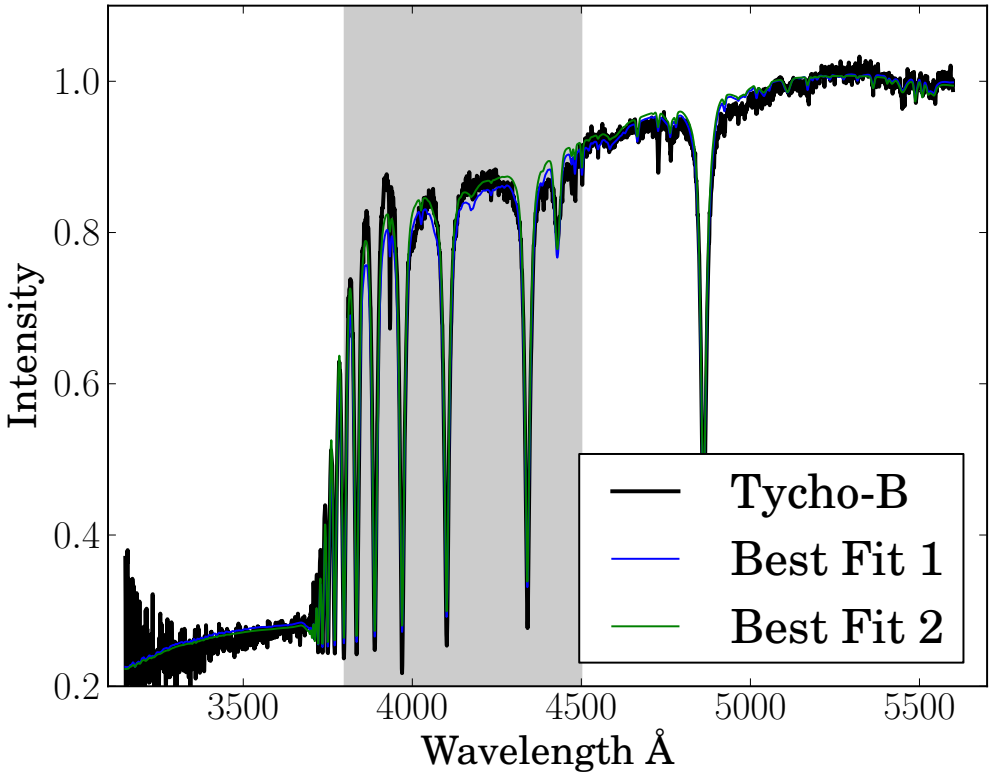

Figure 1.5 The plot shows the normalised spectrum of Tycho-B with the fit which excluded the spectral region between 3800–4500 Å(Best Fit 1) and the fit with the problematic region (Best Fit 2). The region is marked with a grey shade.

Table 1.5 Measured EWs from the Keck HIRES spectra

λ (Å)	χ (eV)	$\log gf$ (dex)	Source[a]	Tycho-A (dex)	Tycho-G (dex)	Tycho-C (dex)	Tycho-E (dex)
5082.35	3.658	-0.59	Reddy03	6.31	6.44		6.2
5088.54	3.85	-1.04	Reddy03	6.19	6.33		
5088.96	3.68	-1.24	Reddy03	6.21			
5094.42	3.83	-1.07	Reddy03	6.1			
5115.4	3.834	-0.28	Reddy03	6.22			
5682.20	4.10	-0.47	RC02	6.34			
5748.351	1.68	-3.26	RC02	6.33		5.74	
5749.297	3.94	-1.99	RC02	6.38			
5847.01	1.676	-3.41	Reddy03	6.26		5.55	
6007.31	1.68	-3.34	RC02	6.2		5.45	
6053.685	4.23	-1.07	RC02	6.33			
6086.28	4.26	-0.52	RC02	6.25	6.22		
6108.116	1.68	-2.44	RC02	6.26	6.11	5.33	
6111.08	4.088	-0.81	Reddy03	6.33		5.38	
6130.14	4.266	-0.94	Reddy03	6.31			
6175.37	4.089	-0.55	Reddy03	6.25	6.35	5.7	
6176.82	4.09	-0.26	Reddy03	6.3	6.27	5.43	6.01
6177.25	1.83	-3.51	Reddy03	6.23			
6186.71	4.10	-0.97	RC02	6.33	6.23		
6204.61	4.09	-1.11	Reddy03	6.32			
6322.17	4.15	-1.17	RC02	6.31			
6370.346	3.54	-1.94	RC02	6.37			
6378.26	4.154	-0.83	Reddy03	6.3		5.81	
6482.80	1.93	-2.63	RC02	6.2		5.38	
6598.60	4.23	-0.98	RC02	6.3		5.74	
6635.12	4.42	-0.83	RC02	6.37			
6643.64	1.68	-2.03	Reddy03	6.48	6.02	5.34	5.97
6767.772	1.83	-2.17	RC02	6.35	6.19	5.67	
6772.32	3.658	-0.97	Reddy03	6.31			
6842.037	3.66	-1.47	RC02	6.4	6.36		
7030.011	3.54	-1.73	RC02	6.42			
7122.197	3.54	0.048	RC02	6.33		5.34	
7261.918	1.95	-2.7	RC02		6.26		
7327.648	3.8	-1.77	RC02	6.38	6.44		
7409.35	3.8	-0.1	RC02			5.24	
7414.502	1.99	-2.57	RC02		6.2	5.57	6.03
7422.275	3.63	-0.129	RC02	6.47		5.32	5.84
7574.048	3.83	-0.58	RC02	6.3	5.97	5.12	
7748.89	3.7	-0.38	Reddy03	6.42	6.17	5.41	6.27
7788.93	1.95	-2.42	RC02			5.87	6.33
7797.59	3.9	-0.35	Reddy03	6.41	6.16	5.59	6.2
7917.44	3.74	-1.5	RC02		6.14		

[a] Reddy et al. (2003) abbrv. as Reddy03; Ramírez & Cohen (2002) abbrv. as RC02

Table 1.6 Tycho-B abundances

Ion designation	λ Å	W_λ Å	ϵ dex	$[X/H]$ dex	$\frac{\partial\epsilon}{\partial\log g}$	$\frac{\partial\epsilon}{\partial T_{\rm eff}}$ K^{-}1
Mg II	4481.13+4481.33	220 ± 15	6.18 ± .08	-1.40	0.08	8×10^{-5}
Si II	6347.1	140 ± 5	6.96 ± .18	-0.59	-0.02	1×10^{-4}
O I	7771.9+7774.2+7775.4	460 ± 30	8.43 ± .10	-0.58	0.24	-4×10^{-5}

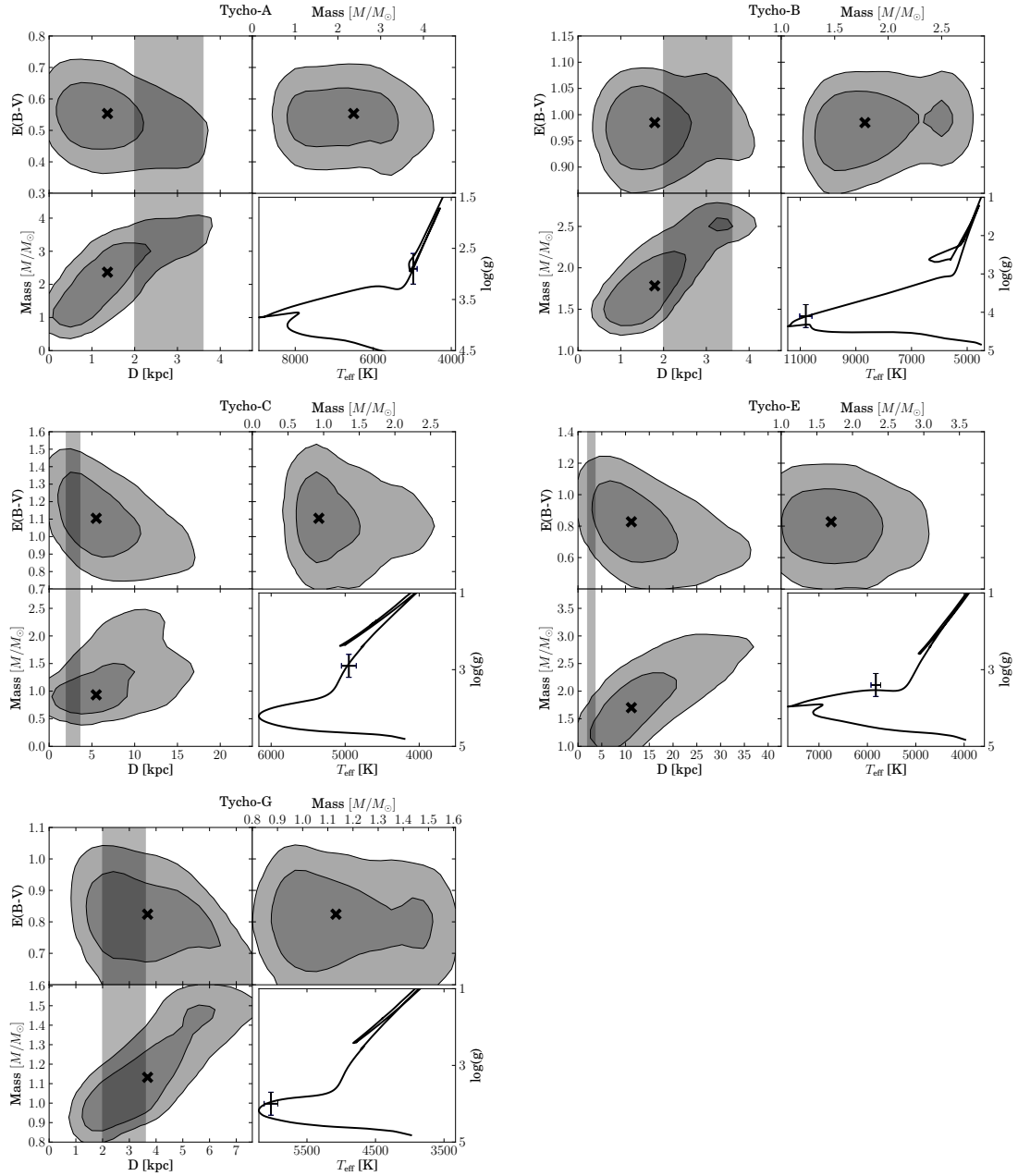

Figure 1.6 The figures show error contours for distance, extinction and mass of the candidates. The lower right shows the optimal isochrone (Pietrinferni et al., 2004) for the measured values of effective temperature and surface gravity.

Table 1.7 Distances, Ages and Masses of candidate stars

Name designation	Mass $M/M_{\odot}$	σ_{Mass} $M/M_{\odot}$	Age Gyr	σ_{Age} Gyr	Distance kpc	$\sigma_{Distance}$ kpc
Tycho-A	2.4	0.8	0.7	2.3	1.4	0.8
Tycho-B	1.8	0.4	0.8	0.3	1.8	0.8
Tycho-C	0.9	0.4	10.0	3.4	5.5	3.5
Tycho-E	1.7	0.4	1.4	1.1	11.2	7.5
Tycho-G	1.1	0.2	5.7	2.1	3.7	1.5

1.4. Discussion

In our sample of six stars we find no star that shows characteristics which strongly indicate that it might be the donor star of SN 1572. On the other hand, it is difficult to absolutely rule out any star, if one is able to invoke improbable post-explosion evolutionary scenarios.

Tycho-A is a metal rich giant. It seems to be likely that Tycho-A is a foreground star. Its principal redeeming feature as a donor star candidate is that it is located in the geometric centre of the remnant, and that it has a relatively low gravity. Tycho-A shows a very low spatial motion which is consistent with a giant donor star scenario, although its lack of rotation is in conflict with a donor star scenario. Taking all measurements into account we regard Tycho-A to be a very weak candidate.

Tycho-B's high temperature, position at the centre of the remnant, high rotational velocity and unusual chemical abundance made it the most unusual candidate in the remnant's centre. Despite the a posteriori unlikely discovery of such a star in the remnant's centre, Tycho-B's high rotational velocity coupled with its low spatial velocity, seem to be in conflict with any viable donor star scenario. These scenarios predict that the donor star will tidally couple to the white dwarf star before explosion, causing the rotation and spatial motion to be correlated post explosion (as discussed in WEK09). The large rotation seen in Tycho-B should accompanied by a large spatial motion, which is ruled out by the observations presented here, a problem we are unable to reconcile with Tycho-B being the donor star.

Tycho-C consists of two stars which are only resolved in HST images. It consists of a brighter bluer component and a dimmer redder component (RP04). In our analysis we find a consistent solution for the spectrum and infer that this is from the bluer brighter component. We find that Tycho-C is a metal-poor giant, probably located beyond the remnant. Tycho-C, similar to Tycho-A might be compatible with a giant donor star scenario. It's lack of rotation and kinematics, however, make it an uncompelling candidate.

Tycho-D is roughly ten times dimmer than the close star Tycho-C ($\approx 0.6''$). Our tools to measure stellar abundances are not effective for spectra with a S/N less than 10. A visual inspection of the star's spectral features shows it to be consistent with a cool star with low rotation. It's brightness precludes it being a relatively slowly rotating giant, and its lack of a fast rotation precludes it being a sub giant or main sequence donor star. All of this suggest Tycho-D is an uncompelling donor candidate star.

Tycho-E is the most distant star in this set (11.2 kpc), although large uncertainties in the distance remain. It seems to be similar to Tycho-G in temperature, but appears to have a lower gravity. It is located $7''$ from the geometric centre, but has no unusual stellar parameters or kinematics. Ihara et al. (2007) have looked at iron absorption lines in stellar spectra made by the remnant and found Tycho-E to be unusual. They suggest that a star in the background would show blue and redshifted iron lines, whereas a star inside the remnant would only show blueshifted iron lines, and a foreground star will not show any iron features from the remnant. Ihara et al. (2007) suggest that Tycho-E only shows blue-shifted lines and thus is suggested as being in the remnant. We believe however that Tycho-E is located far behind the remnant and suggest that a low column density on the receding side of the remnant could cause a lack of red-shifted iron features. In summary, a lack of rotation, kinematic signatures, and an inconsistent distance make Tycho-E a very weak candidate.

Tycho-G is located 30″ from the X-ray centre which makes it the most remote object to the centre in this work. This work confirms the radial velocity measured by GH09 and WEK09. Figure 1.2 shows the expected distribution of radial velocities from the Bescançon model of Galactic dynamics. Tycho-G lies well within the expect range of radial velocity for stars with its stellar parameters and distance. In addition, this work has analysed the proper motion of stars around the centre of SN 1572. Figure 1.1 shows Tycho-G to have a marginally significant proper-motion measurement. However, these proper motion measurements show other outliers at a rate higher than expect by Galactic models (Besançon), to study this difference we have selected candidates within a 1° radius around SN 1572 from the proper motion catalogue PPMXL (Roeser et al., 2010). To exclude the many foreground stars we have introduced the additional selection criteria $R > 16$ and $V - R < 1$ (the sun has a colour of $V - R = 1.3$). Using these same selection criteria on the Besançon Model resulted in 95% of stars more distant than 2 kpc. This set shows stars with similarly high proper motions like Tycho-G are relatively common - it is not unexpected to have a star with Tycho-G's motion inside the remnant's centre (see Figure 1.7). We conclude that the Besançon Model, although a good rough estimate, does not provide a detailed overview of proper motion space, and it is more appropriate to compare to the PPMXL catalog. Finally, the HST proper motion measurements are challenging, and there might be systematic errors in our proper motion measurements which are larger than our reported statistical errors. The errors tend to increase the chance of larger than actual proper motion measurements. Taken in total, while Tycho-G may have an unusual proper motion, the significance of this motion, even if current measurements are exactly correct, is not exceptional. As described, the kinematic features of a donor star might easily be lost in the kinematic noise of the Galaxy. WEK09, however, suggested using post-explosion stellar rotation as a possible feature for a donor star. This work suggests that Tycho-G has a rotation below the instrumental profile of 6 km s^{-1}.

We find Tycho-G to be a subgiant/main sequence star with roughly solar temperature and metallicity. GH09 measure a slight nickel enhancement, which they believe to originate in the contamination from the ejecta. Figure 1.4 compares our measurement of Tycho-G to the distribution of nickel (see Figure 1.4) and we find it to be consistent. In addition, we could not measure a significantly enhanced lithium-abundance as suggested in GH09. Finally, we have measured the distance to Tycho-G and find that most likely Tycho-G lies behind the remnant, although the range of uncertainties includes the remnant distance.

In summary, Tycho-G may have unusual kinematics as indicated by its proper motion, the significance of this motion is not large when compared to a large sample of similar stars in the direction of the Tycho remnant. Furthermore, such a kinematic signature, if it were related to the binary orbital velocity, predicts rotation for Tycho-G which we do not observe (modulo the weak caveats from WEK09). Furthermore, we have not found a reasonable explanation for Tycho-G's large distance to the geometric centre, and suggest that Tycho-G is unlikely to be related to the Tycho SNR.

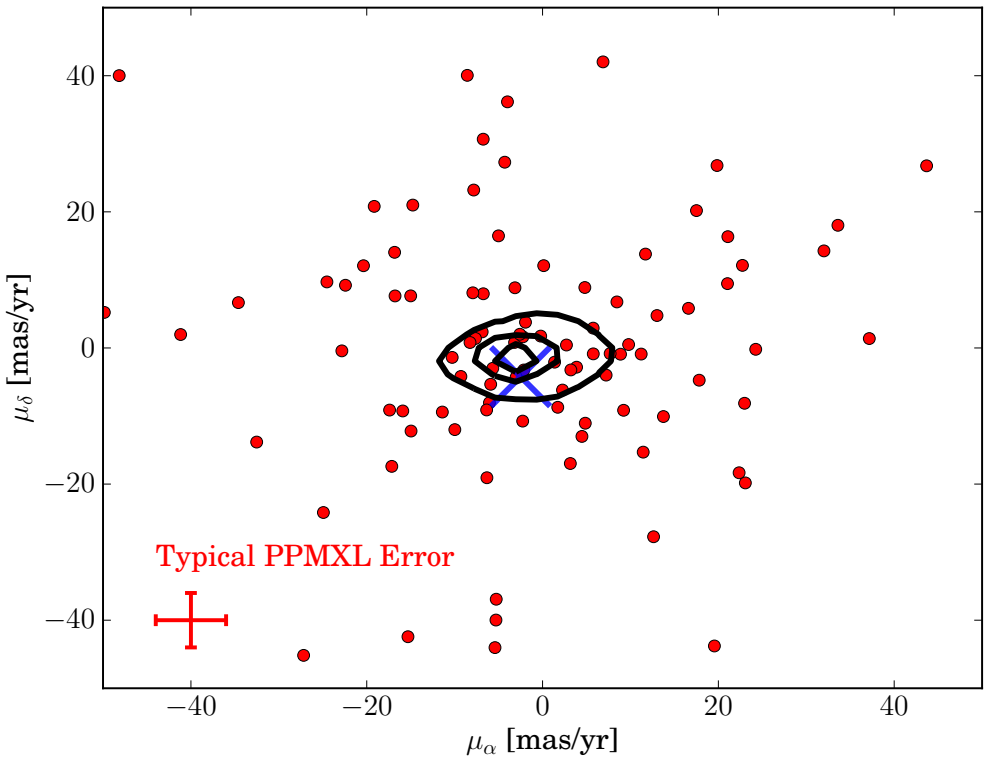

Figure 1.7 example caption

1.5. Conclusion

This work did not detect an unambiguously identifiable donor star candidate. Although stars Tycho-B and Tycho-G have unusual features, there remains no convincing explanation for all of their parameters which can be attributed to the donor star scenario. Further theoretical predictions are needed to make a more precise distinction between donors and unrelated stars.

Our observations provide a case that the Tycho SNR does not have a main sequence, sub giant, or red giant donor star, but other possibilities remain. These include a helium donor, such as the so-called sub Chandrasekhar Mass explosions discussed by Livne & Arnett (1995); Sim et al. (2010). These progenitor systems might leave behind a very faint and fast moving helium star, or no remnant at all (priv. comm. Rüdiger Pakmor) . Such a progenitor would probably evade detection, and would likely not leave behind traces, such as circumstellar interaction (CSI) with the remnant, or early light curve anomalies (Kasen, 2010). However, deep multi-epoch wide field optical images should catch any such star speeding away from the remnant centre - these are observation not yet taken. Finally, a double degenerate progenitor, in most cases, does not leave behind a remnant , and is consistent with finding no donor star in SNR 1572.

SN 1006 and SN 1604 (Kepler's SN) are two other SN Ia remnants in the Milky Way. SN 1006 is far from the plane and shows no signs of CSI. SNR 1604 while far from the galaxy plane, shows CSI with its remnant, and has all the indications of what might be

expected from a SD-Scenario with an AGB donor (Chiotellis et al., 2011). Observations of these remnant will better establish if there is a continued pattern to the unusual stars in SN Iaremnant centres, or whether the lack of viable donor stars persists in multiple systems.

Bibliography

Anderson, J., & King, I. R. 2006, PSFs, Photometry, and Astronomy for the ACS/WFC, Tech. rep. (ADS entry)

Asplund, M., Grevesse, N., Sauval, A. J., & Scott, P. 2009, ARA&A, 47, 481 (ADS entry)

Badenes, C., Borkowski, K. J., Hughes, J. P., Hwang, U., & Bravo, E. 2006, ApJ, 645, 1373 (ADS entry)

Beals, C. S., & Blanchet, G. H. 1937, PASP, 49, 224 (ADS entry)

Bessell, M. S. 2007, PASP, 119, 605 (ADS entry)

Bianco, F. B., et al. 2011, ArXiv e-prints (ADS entry)

Castelli, F., & Kurucz, R. L. 2003, in IAU Symposium, Vol. 210, Modelling of Stellar Atmospheres, ed. N. Piskunov, W. W. Weiss, & D. F. Gray, 20P–+ (ADS entry)

Castelli, F., & Kurucz, R. L. 2004, ArXiv Astrophysics e-prints (ADS entry)

Chandrasekhar, S. 1931, ApJ, 74, 81 (ADS entry)

Chiotellis, A., Schure, K. M., & Vink, J. 2011, ArXiv e-prints (ADS entry)

Dan, M., Rosswog, S., Guillochon, J., & Ramirez-Ruiz, E. 2011, ArXiv e-prints (ADS entry)

Fink, M., Röpke, F. K., Hillebrandt, W., Seitenzahl, I. R., Sim, S. A., & Kromer, M. 2010, A&A, 514, A53+ (ADS entry)

Foley, R. J., et al. 2003, PASP, 115, 1220 (ADS entry)

González Hernández, J. I., Ruiz-Lapuente, P., Filippenko, A. V., Foley, R. J., Gal-Yam, A., & Simon, J. D. 2009, ApJ, 691, 1 (ADS entry)

Han, Z. 2008, ApJ, 677, L109 (ADS entry)

Hayden, B. T., et al. 2010, ApJ, 722, 1691 (ADS entry)

Heiter, U., et al. 2002, A&A, 392, 619 (ADS entry)

Herbig, G. H. 1966, ZAp, 64, 512 (ADS entry)

Herbig, G. H. 1967, in IAU Symposium, Vol. 31, Radio Astronomy and the Galactic System, ed. H. van Woerden, 85–+ (ADS entry)

—. 1975, ApJ, 196, 129 (ADS entry)

—. 1995, ARA&A, 33, 19 (ADS entry)

Hibbins, R. E., Miles, J. R., Sarre, P. J., & Herbig, G. H. 1994, in The Diffuse Interstellar Bands, ed. A. G. G. M. Tielens, 31–+ (ADS entry)

Horne, K. 1986, PASP, 98, 609 (ADS entry)

Hughes, J. P. 2000, ApJ, 545, L53 (ADS entry)

Ihara, Y., Ozaki, J., Doi, M., Shigeyama, T., Kashikawa, N., Komiyama, K., & Hattori, T. 2007, PASJ, 59, 811 (ADS entry)

James, F., & Roos, M. 1975, Comput. Phys. Commun., 10, 343

Jeffery, C. S., Woolf, V. M., & Pollacco, D. L. 2001, A&A, 376, 497 (ADS entry)

Jenniskens, P., & Desert, F. 1994, A&AS, 106, 39 (ADS entry)

Kasen, D. 2010, ApJ, 708, 1025 (ADS entry)

Kerzendorf, W. E., Schmidt, B. P., Asplund, M., Nomoto, K., Podsiadlowski, P., Frebel, A., Fesen, R. A., & Yong, D. 2009, ApJ, 701, 1665 (ADS entry)

Kobayashi, C., Umeda, H., Nomoto, K., Tominaga, N., & Ohkubo, T. 2006, ApJ, 653, 1145 (ADS entry)

Krause, O., Tanaka, M., Usuda, T., Hattori, T., Goto, M., Birkmann, S., & Nomoto, K. 2008, Nature, 456, 617 (ADS entry)

Kupka, F. G., Ryabchikova, T. A., Piskunov, N. E., Stempels, H. C., & Weiss, W. W. 2000, Baltic Astronomy, 9, 590 (ADS entry)

Kurucz, R., & Bell, B. 1995, Atomic Line Data (R.L. Kurucz and B. Bell) Kurucz CD-ROM No. 23. Cambridge, Mass.: Smithsonian Astrophysical Observatory, 1995., 23 (ADS entry)

Leonard, D. C. 2007, ApJ, 670, 1275 (ADS entry)

Livne, E., & Arnett, D. 1995, ApJ, 452, 62 (ADS entry)

Matheson, T., Filippenko, A. V., Ho, L. C., Barth, A. J., & Leonard, D. C. 2000, AJ, 120, 1499 (ADS entry)

Mennekens, N., Vanbeveren, D., De Greve, J. P., & De Donder, E. 2010, A&A, 515, A89+ (ADS entry)

Munari, U., Sordo, R., Castelli, F., & Zwitter, T. 2005, A&A, 442, 1127 (ADS entry)

Nelemans, G. 2010, http://www.lorentzcenter.nl/lc/web/2010/391/presentations/Nelemans.pdf

Oke, J. B., Cohen, J. G., Carr, M., et al. 1995, PASP, 107, 375 (ADS entry)

Pakmor, R., Kromer, M., Röpke, F. K., Sim, S. A., Ruiter, A. J., & Hillebrandt, W. 2010, Nature, 463, 61 (ADS entry)

Patat, F., et al. 2007, Science, 317, 924 (ADS entry)

Pietrinferni, A., Cassisi, S., Salaris, M., & Castelli, F. 2004, ApJ, 612, 168 (ADS entry)

Pinto, P. A., et al. 2006, in Bulletin of the American Astronomical Society, Vol. 38, American Astronomical Society Meeting Abstracts, 1017–+ (ADS entry)

Ramírez, S. V., & Cohen, J. G. 2002, AJ, 123, 3277 (ADS entry)

Reddy, B. E., Tomkin, J., Lambert, D. L., & Allende Prieto, C. 2003, MNRAS, 340, 304 (ADS entry)

Rest, A., et al. 2008, ApJ, 681, L81 (ADS entry)

Reynoso, E. M., Moffett, D. A., Goss, W. M., Dubner, G. M., Dickel, J. R., Reynolds, S. P., & Giacani, E. B. 1997, ApJ, 491, 816 (ADS entry)

Robin, A. C., Reylé, C., Derrière, S., & Picaud, S. 2003, A&A, 409, 523 (ADS entry)

Roeser, S., Demleitner, M., & Schilbach, E. 2010, AJ, 139, 2440 (ADS entry)

Ruiter, A. J., Belczynski, K., & Fryer, C. 2009, ApJ, 699, 2026 (ADS entry)

Ruiz-Lapuente, P. 2004, ApJ, 612, 357 (ADS entry)

Ruiz-Lapuente, P., et al. 2004, Nature, 431, 1069 (ADS entry)

Saio, H., & Nomoto, K. 1985, A&A, 150, L21 (ADS entry)

Sim, S. A., Röpke, F. K., Hillebrandt, W., Kromer, M., Pakmor, R., Fink, M., Ruiter, A. J., & Seitenzahl, I. R. 2010, ApJ, 714, L52 (ADS entry)

Sneden, C. 1973, ApJ, 184, 839 (ADS entry)

Tonry, J., & Davis, M. 1979, AJ, 84, 1511 (ADS entry)

Tucker, B. E. 2011, Ap&SS, 40 (ADS entry)

Vogt, S. S., et al. 1994, in Presented at the Society of Photo-Optical Instrumentation Engineers (SPIE) Conference, Vol. 2198, Society of Photo-Optical Instrumentation Engineers (SPIE) Conference Series, ed. D. L. Crawford & E. R. Craine, 362–+ (ADS entry)

Warren, J. S., et al. 2005, ApJ, 634, 376 (ADS entry)

Wilson, R. 1958, ApJ, 128, 57 (ADS entry)

Yong, D., Lambert, D. L., Paulson, D. B., & Carney, B. W. 2008, ApJ, 673, 854 (ADS entry)

Yu, S., & Jeffery, C. S. 2010, A&A, 521, A85+ (ADS entry)